Review of Analysis and Modeling Techniques for Incompressible, Turbulent Bluff-Body Wakes

Logan D. Halstrom* and Federico Zabaleta†
University of California, Davis, California, 95616

abstract here *LH&FZ*

Nomenclature

α	=	Angle of Attack, deg
ρ	=	density, kg/m^3
Re	=	Reynolds Number, N.D.
Subscripts		
$()_\infty$	=	freestream quantity
D	=	Diameter as reference length
Acronyms		
CFD	=	Computational Fluid Dynamics
RANS	=	Reynolds-Averaged Navier-Stokes
URANS	=	Unsteady Reynolds-Averaged Navier-Stokes
SAS	=	Scale-Adaptive Simulation
LES	=	Large Eddy Simulation
DES	=	Detached Eddy Simulation
ZDES	=	Zonal Detached Eddy Simulation
DDES	=	Delayed Detached Eddy Simulation
DNS	=	Direct Numerical Simulation

I. Introduction

BODIES When a body moves in a fluid, it experience different forces, such as lift and drag. Drag can occur due to a difference in velocity in the surface of the body and the mean flow, in which case we call it friction drag. This friction is associated with the development of boundary layers and is it scales with the Reynolds number. If the drag is due to a difference in pressure trough the surface of the body, then we call it pressure drag or viscous induced drag.

*Graduate Student, Mechanical And Aerospace Engineering Department, One Shields Avenue
†Graduate Student, Civil and Environmental Engineering Department, One Shields Avenue

This drag is usually associated with separation of the flow and the formation of a wake downstream the body. In real flows, drag is composed by the combination of both. The effect of frictional drag is usually more relevant for attached flows while the pressure drag prevails in separated flows.

We can analyze the effect of friction and pressure drag by analyzing the flow around a flat plate. If the flat plate is oriented in the direction of the flow, then the friction drag will be important while the pressure drag will be almost negligible. On the other side, if the orient the flat plate perpendicular to the flow, then the difference of pressure between both sides of the plate will be much more important than the effect of the friction, and so the pressure drag will be dominant.

When the drag of a body is dominated by viscous drag, we define the body as a streamlined body. Flat plates (oriented in the direction of the flow) or airfoils with a small angle of attack are examples of those. When the flow is dominated by pressure drag, we define the body as a bluff or blunt body. Examples or these are squares, cylinders, spheres or airfoil at large angle of attack. Whether a body is considered bluff or streamlined is only a function of its shape and its orientation with respect to the flow.

INSERT FIGURE

- Driving Physical Phenomena *FZ*
  - differences from potential flow
  - blunt/bluff body definition, differences from streamlined body flow
  - massively separated flow
  - base pressure
  - wake
- Real World Applications *LH*
  - parachute
  - reentry capsule
  - vehicles
  - buildings
  - show similarity between cylinder/sphere wake and more complex bluff body
  - relevance: stability, acoustics, buffeting/unsteady loads, mixing

Bluff-body flow is applicable to a plethora of real-world applications. Massively separated wakes are characterized by complex, unsteady, and sometime unstable turbulent phenomena, which can lead to design concerns throughout the fields of engineering. A few examples of bluff-body flow in engineering applications include wall-mounted cubes representative of a high-rise buildings [1], bridge spans [2] as modeled in Fig 1, ground vehicles [3] like the passenger sedan shown in Fig 3, atmospheric reentry vehicles [4] like the Orion wind tunnel model in Fig 2, humans in ejection seats and parachutes, both demonstrated in Fig 2, aircraft protuberances such as landing-gear trucks, space launch vehicles, and flame holders [5] in combustors Fig 4.

Bluff-bodies are common in civil engineering applications, where engineers might be concerned in predicting unsteady wind loading leading to structural resonance, which was a major design flaw for the Tacoma Narrows Bridge. Fig 1 demonstrates a model bridge span undergoing wake-induced vibration due to the vortex shedding caused by the gap in the center [2].

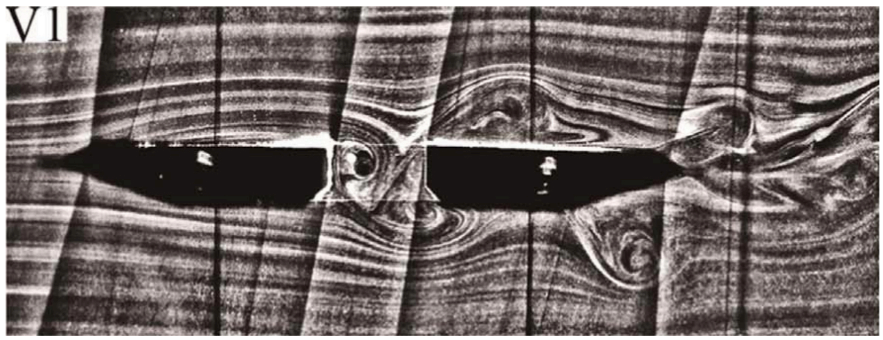

Fig. 1 Instantaneous PIV flow field of bridge model similar to Tacoma Narrows bridge (Re=587) [2]

Unsteady loading and buffeting can also be a potentially catastrophic bluff-body wake effect for mechanical and aerospace engineering applications. The dynamic situation of a cockpit emergency egress system as depicted in Fig 2 requires precise understanding of the unsteady forces on the ejection seat and human in order to mitigate any injuries the escaping pilot might experience.

Fig. 2 Left: Mk-16 ejection seat rocket sled test (Martin-Baker), Right: Shadowgraph wake of Orion capsule model ($M = 0.3, \alpha = 29.25^o, Re_D = 5.3 \times 10^6$) [4]

Dynamic stability can also be adversely affected by bluff-body wake behavior. The drogue parachute in Fig 2 and the model Orion capsule in Fig 2 are both situations where dynamic instability of the bluff-body could lead to potentially fatal situations for the humans involved.

Acoustics can also be a design concern either due to unsteady loading as in the case of a launch vehicle or due to noise concerns or restrictions such as those for aircraft noise. Even passenger vehicles such as that shown in Fig 3 can create a separated wake which could lead to acoustic disturbance of the passengers inside.

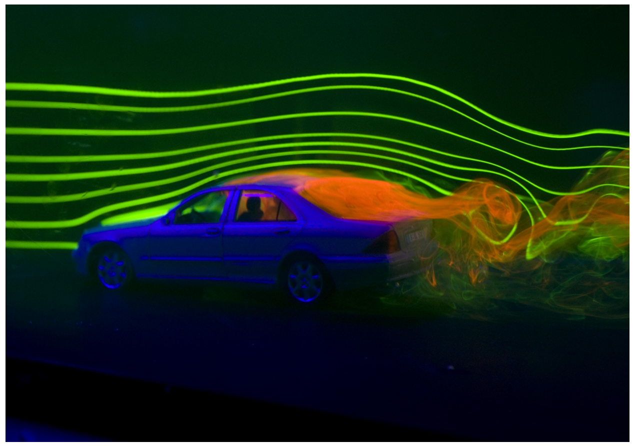

Fig. 3 Streamlines and separated flow over a car in a wind tunnel (NASA/Eric James)

There are even applications for bluff-bodies outside the concepts of loading and acoustics. In industrial applications where a high-speed mixture must be ignited, it is necessary to both reduce the speed and mix the flow around an ignition source to allow a flame to stabilize. This effect can be created by placing a triangular bluff-body directly upstream of an ignitor such that its recirculation region entrains slower-moving mixture at the ignitor's location (Fig 4) [6].

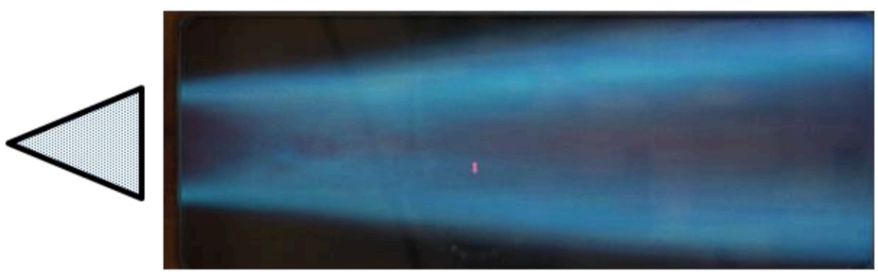

Fig. 4 Image of a stabilized flame held in the wake of a bluff-body flame holder [5]

Big whorls have little whorls, which feed on their velocity, and little whorls have lesser whorls, and so on to viscosity (in the molecular sense). Richardson (1922) [7]

II. Flow around a bluff body and transition

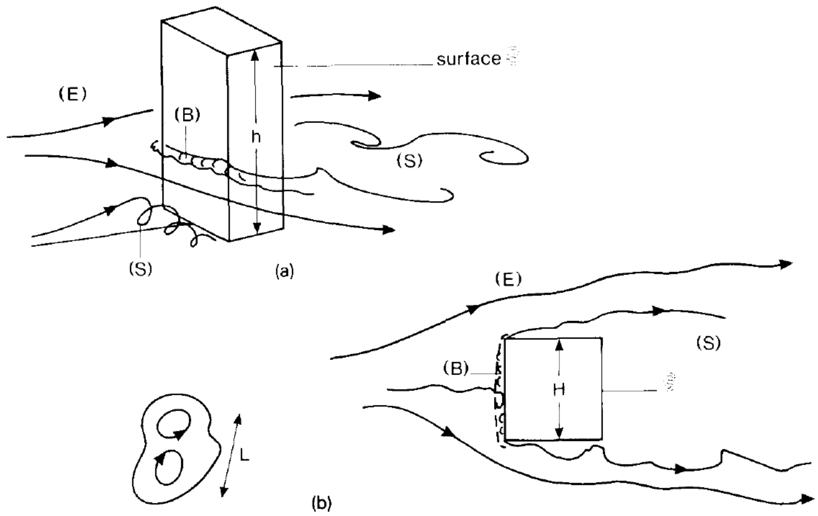

Fig. 5 Regions of disturbed flow. Extracted from [8]

A. Steady laminar wake

B. Periodic Laminar Regime

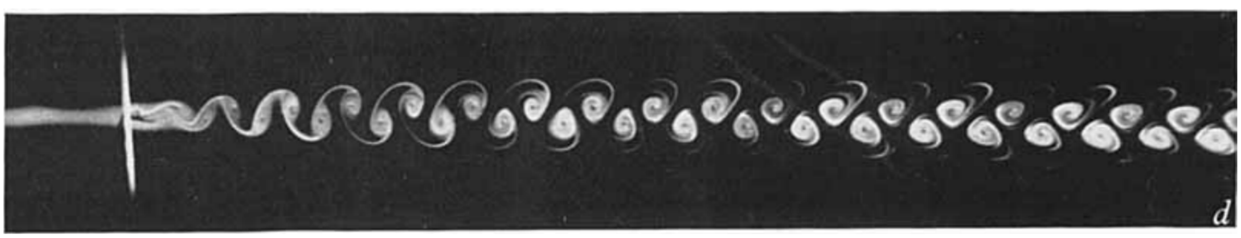

Fig. 6 Kárman-Bénard eddy street at *Re = 100*. Extracted from [9]

C. Transition in wake state

Fig. 7 Transition in wake at *Re = 190*. Extracted from [9]

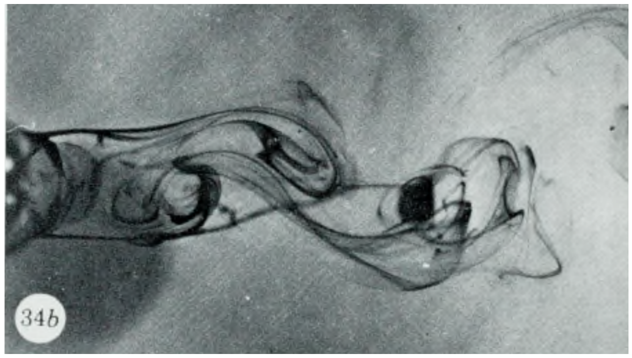

Fig. 8 Transition in wake at *Re = 344*. Extracted from [10]

D. Transition in shear layers state

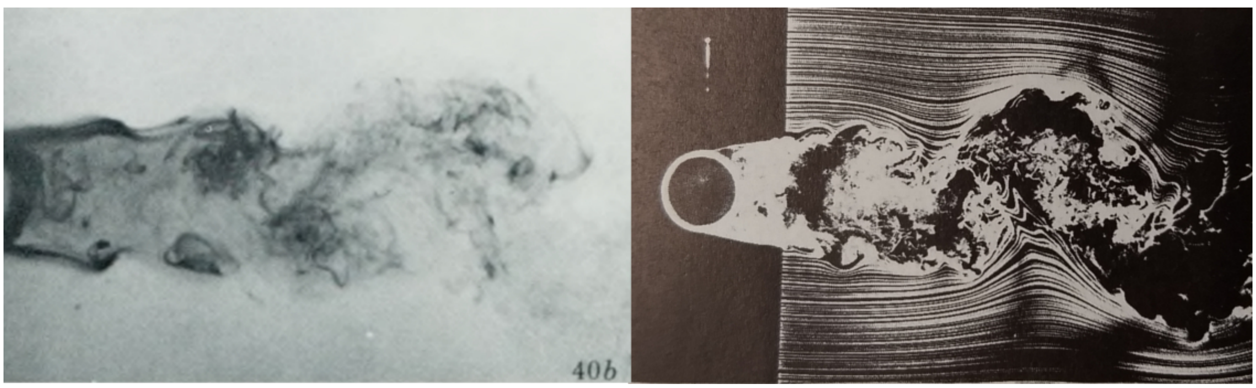

Fig. 9 Transition in free shear layer. Left: *Re = 1083*. Extracted from [10]. Right: *Re = 8000*. Extracted from [11]

E. Transition in boundary layer

F. Fully turbulent state

III. Free stream turbulence and non-uniform free stream

IV. Experimental Methods And Results

FZ

- Historical Study
- Experimental techniques
  - ballistic range?
- Applications
  - Simple cases: cylinder/sphere

    * Drag vs Re?
    * Wake velocity profiles?
    * Wake structure?
  - Sharp vs bluff: sphere vs cube
  - Complex cases: capsule/building

V. Computational Methods and Results

LH

- Historical Study
- Computational techniques
- Applications
  - Simple cases: cylinder/sphere
  - Sharp vs bluff: sphere vs cube
  - Complex cases: capsule/building

A. Turbulence Modeling Aspects

LH

- Brief turbulence model description
  - RANS vs URANS
  - DNS
  - LES (uses DNS) and DES (=Hybrid RANS/LES)
- Compare turbulence model performance for sphere/cylinder
  - DES > URANS > RANS
  - DES = functional LES
  - SAS vs DES?
  - DNS: limited Re
- Shortcomings of each model (and how to address them)
  - URANS
  - DES: only good at sharp separation
    * "An order of accuracy has not even been proposed for a simulation using both modes within DES" -Spalart about hybrid method
    * grid induced separation (maybe not an issue for bluff bodies)
    * DES can default to RANS if grid adaptation misses a shear layer

* more computational cost than RANS

- Advanced geometries
  - f-15
  - car
  - building
  - capsule
  - chute, landing gear, helicopter, wind turbine

LIST ALL FIGURES HERE, REORDER AND DESCRIBE LATER

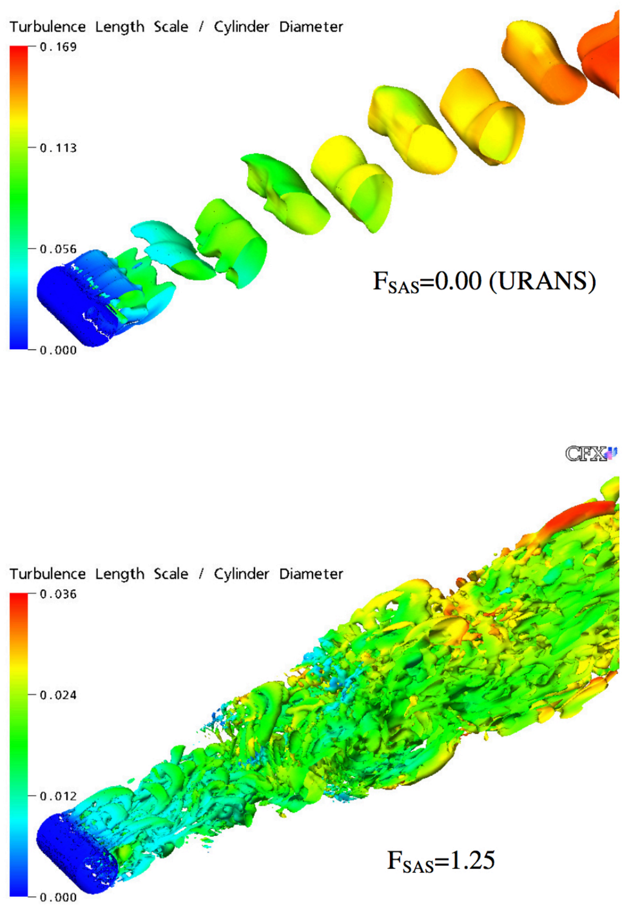

Fig. 10 SAS vs URANS cylinder [12]

Figure 5: Resolved structures for cylinder in crossflow using different constants FSAS Re=3.6e6

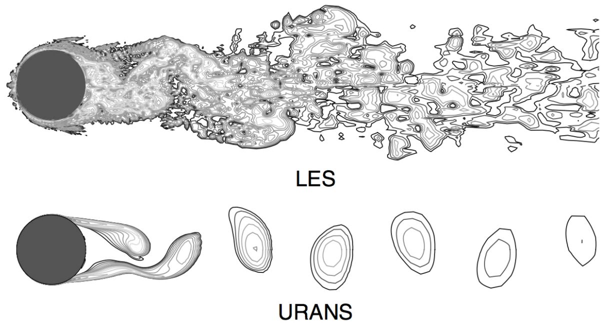

Fig. 11 cylinder les vs urans instantaneous [13]

Instantaneous vorticity magnitude at a given spanwise cut for flow over a circular cylinder at ReD 1⁄4 1 106. 25 contour levels from xD=U1 1⁄4 1 to xD=U1 1⁄4 575 (exponential distribution) are plotted.

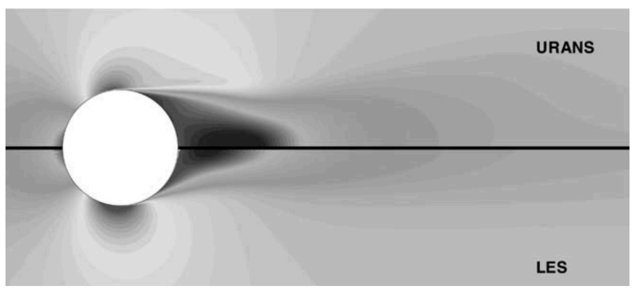

Fig. 12 cylinder les vs urans averaged [13]

Fig. 5. Mean streamwise velocity distribution predicted by LES and URANS. 45 contour levels from U=U1 1⁄4 0:2 to U=U1 1⁄4 1:7 are plotted.

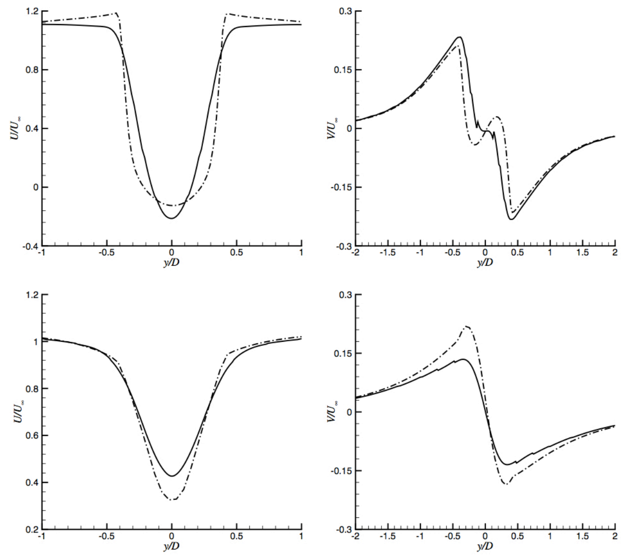

Fig. 13 cylinder les vs urans velocity profiles [13]

Fig. 6. Mean streamwise and vertical velocities at x=D 1⁄4 0:75 (upper figures) and x=D 1⁄4 1:50 (lower figures): (—) LES; (– –) URANS

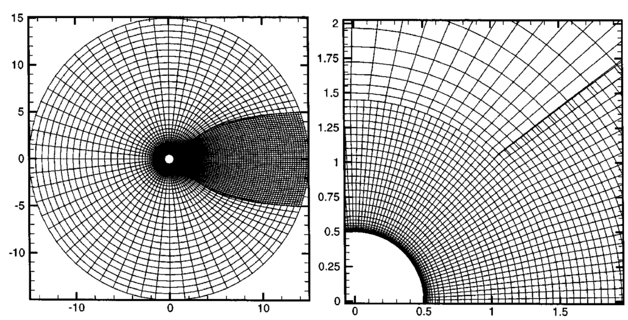

Fig. 14 cylinder les vs rans grid [14]

Figure1. Medium computational grid, CaseTS2.Innerblock150×36,wakeblock74×36, outer block 59 × 30. The three blocks meet near x = 1.06, y = 1.03. Grid for spalart cylinders.

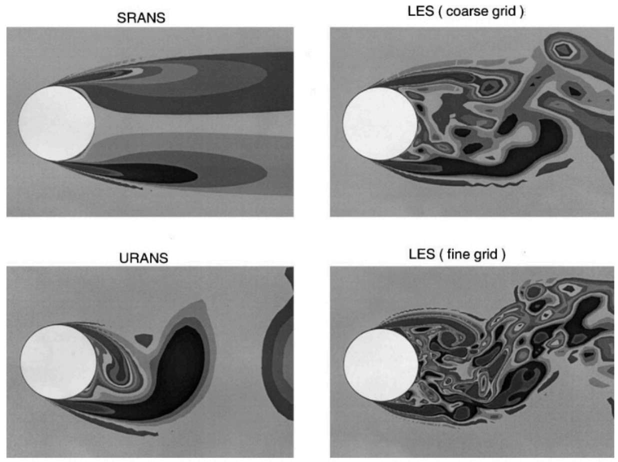

Fig. 15 cylinder les vs rans [15]

grid for LES shown above (actual simulations were DES)

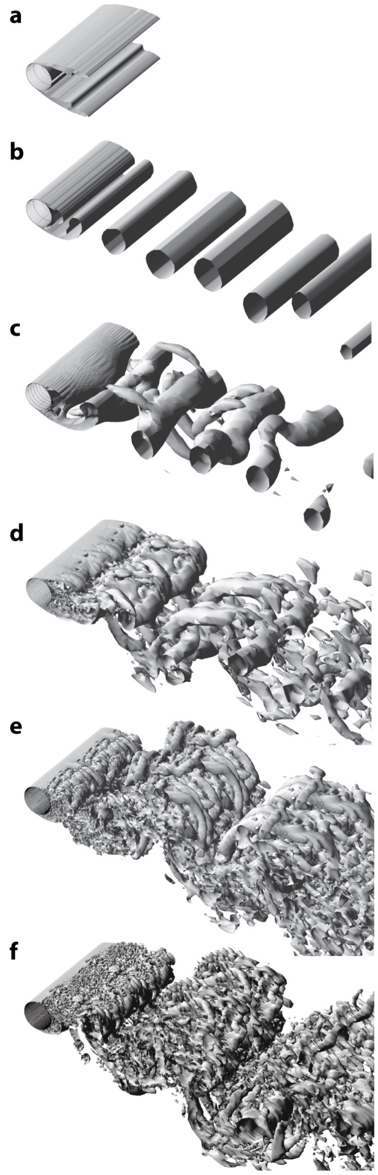

AR Spalart PR. 2009.
Annu. Rev. Fluid Mech. 41:181–202

Fig. 16 cylinder simulation with RANS, 2DURANS, 3DURANS, SSTDES, SADES [16]

Vorticity isosurfaces by a circular cylinder: ReD = 5 × 104, laminar separation. Experimental drag coefficient Cd = 1.15–1.25. (a) Shear-stress transport (SST) turbulence model steady Reynolds-averaged Navier-Stokes (RANS), Cd = 0.78; (b) SST 2D unsteady RANS, Cd = 1.73; (c) SST 3D unsteady RANS, Cd = 1.24; (d) Spalart-Allmaras (SA) detached-eddy simulation (DES), coarse grid, Cd = 1.16; (e) SA DES, fine grid, Cd = 1.26; (f) SST DES, fine grid, Cd = 1.28. Figure courtesy of A. Travin

illustrates the response of DES to grid refinement in its LES region.

DES solutions with different base RANS models are not sensitive to model choice in the LES region (as opposed to the RANS region, particularly if separation occurs).

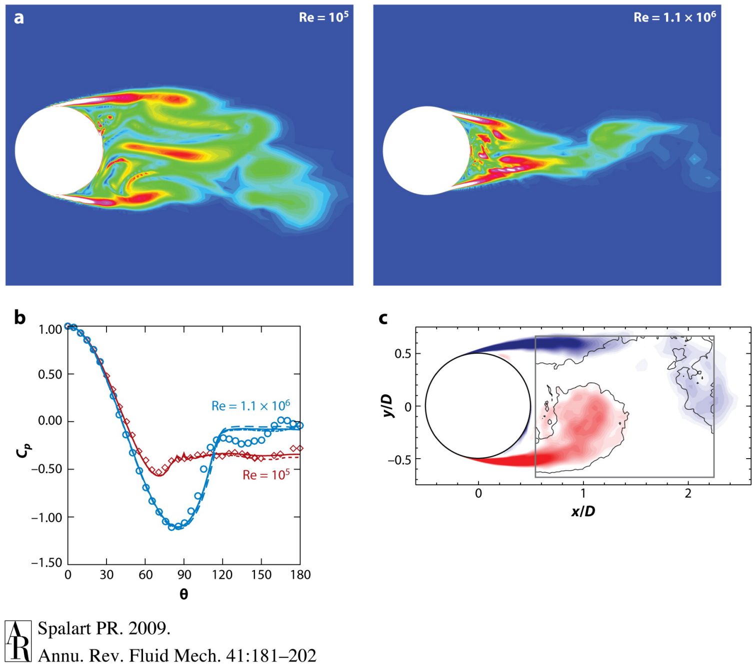

Fig. 17 DES validation from [16]. Sphere transition and drag crisis from [17]. Vorticity validation from [18]

Simple bluff bodies. (a) Flow visualizations and (b) pressure distributions for a sphere. Re = 105 and 1.1 × 106. Open circles and diamonds denote experiments, whereas the dotted and dashed lines denote detached-eddy simulation (DES) on two grids. Panels a and b courtesy of K. Squires. (c) Phase-averaged vorticity contours for a cylinder. Color gradations denote DES conducted by Mockett et al. (2008), and the solid line denotes experiments by the same authors.

NOTE: DES could be used to emulate the dimples on a golf ball by setting the boundary layer separation point, but true simulation of flow in golf ball dimples requires DNS due to the range of scales

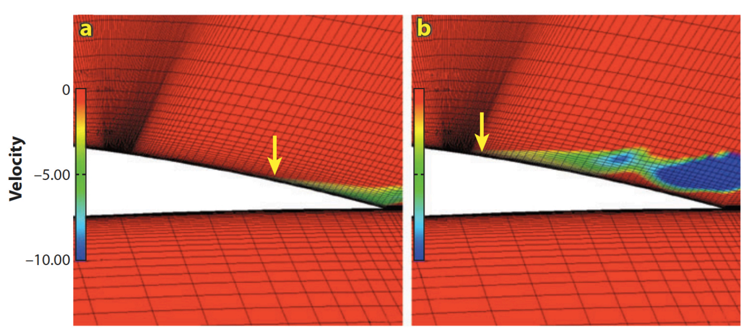

Fig. 18 Example of DES grid induced separation from [16], source: [19]

Vorticity contours over an airfoil: (a) Reynolds-averaged Navier-Stokes and (b) detached-eddy simulation. Arrows indicate separation. Figure taken from Menter & Kuntz 2002.

Potential con of using DES. EXPLAIN HOW GRID INDUCED SEPARATION WORKS.

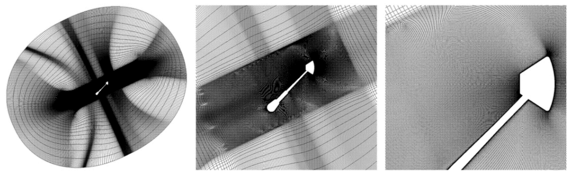

Fig. 19 Orion capsule grid [20]

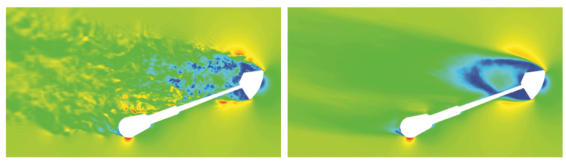

Fig. 20 Orion capsule mach number instantaneous (left) time-averaged (ight) (DES, M=0.5) [20]

Plots of Mach number for an instantaneous and time-averaged solution. For an illustration of the amount of unsteadiness this removed, refer to Fig. 6. It shows a slice of Mach number through the pitch plane (fi 0 deg) for a DES–KEC solution at Mach 0.50, AoA 170 deg.

RANS did ok compared to WTT/DES for some cases but in others, DES outperformed

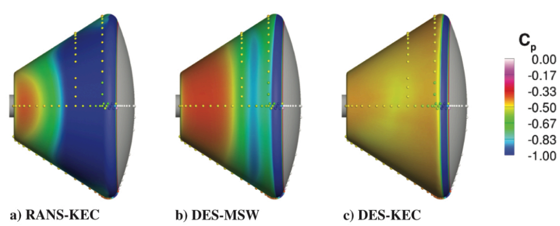

Fig. 21 surface pressure comparison of RANS, DES, WTT, M=0.5 [20]

Freckle plots of pressure tap data, viewed from fi 180 deg, for Mach 0.50, AoA 155 deg case

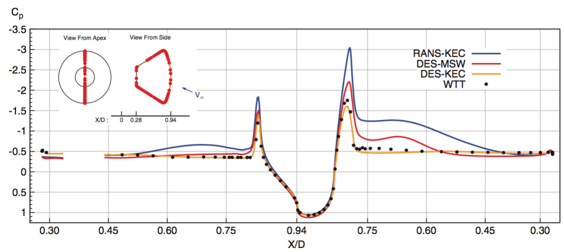

Fig. 22 surface pressure tap comparison of RANS, DES, WTT, M=0.5 [20]

Line plots of pressure tap for data Mach 0.50, AoA 155 deg case.

RANS fails to predict suction peak, surface pressures in wake. Gets best lift integration compared to DES due to separation prediction, worse drag due to wake pressure prediction.

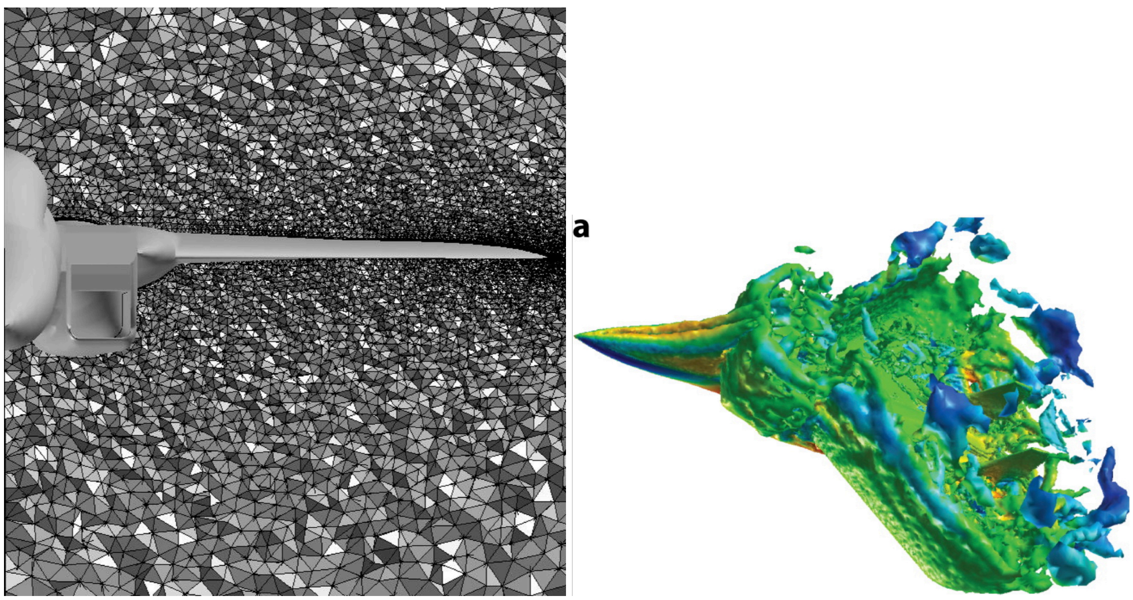

Fig. 23 F-15 DES grid (left) [21] vorticity isocontours (right) [16]

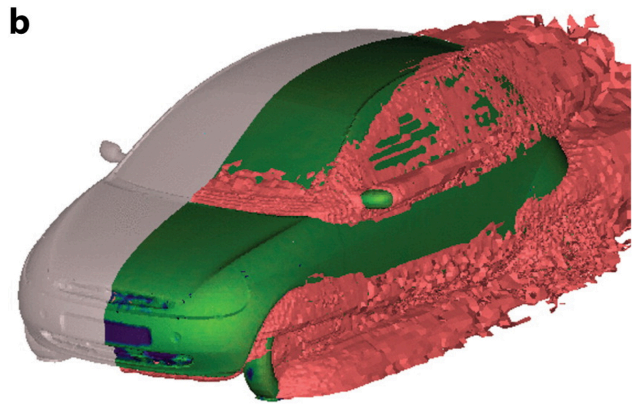

Fig. 24 car DES isocontours [3]

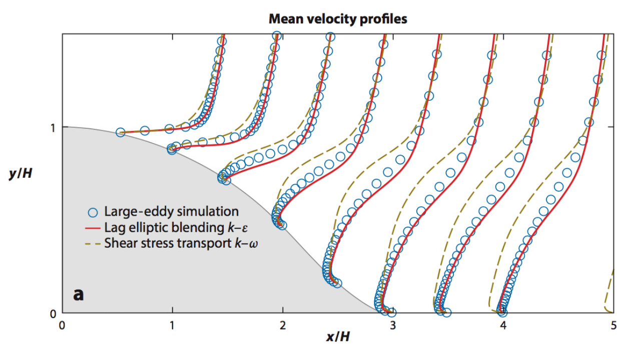

Fig. 25 curve backstep velocity profile les vs rans [22]

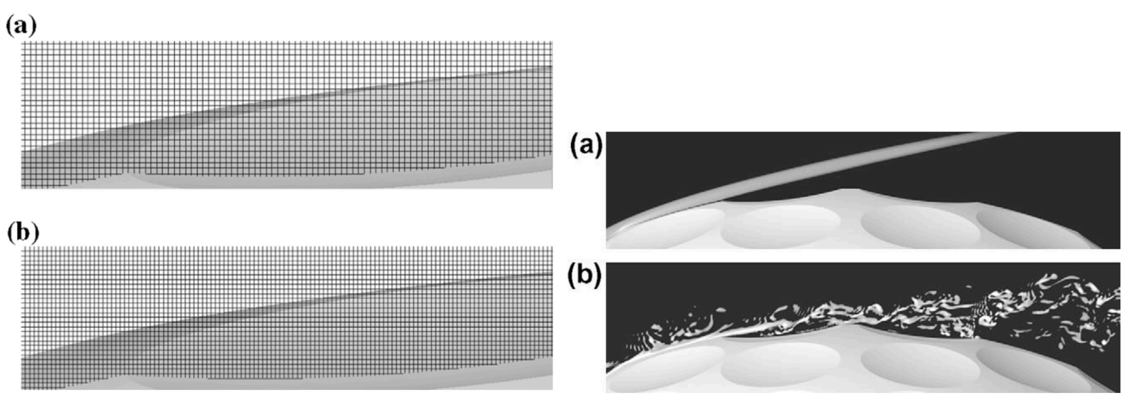

Fig. 26 DNS non-rotating golf ball with dimples grid (left) vorticity (right) [23]

Example grid resolution in a dimple near 84° (measured from the stagnation point at the front of the golf ball). (a) Re = 2.5 104; (b) Re = 1.1 105.

Contours of azimuthal vorticity. (a) Re = 2.5 104; (b) Re = 1.1 105

NOTE: Recall sphere example from Spalart review and say that this is the analogous DNS experiment to his DES

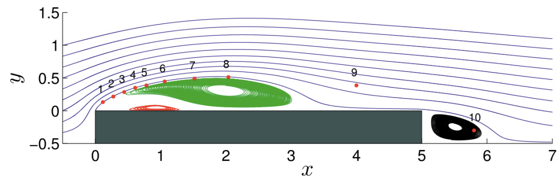

Fig. 27 DNS square cylinder vortex locations Re=3000 [24]

Fig. 4. Streamlines of the mean velocity field (U,V) (x,y) The green lines show the primary vortex, the red lines mark the secondary vortex and the black lines denote the wake vortex. The red dots denote the locations of the probes used for the computation of time spectra in section x5. (For interpretation of the references to color in this figure legend, the reader is referred to the Web version of this article.)

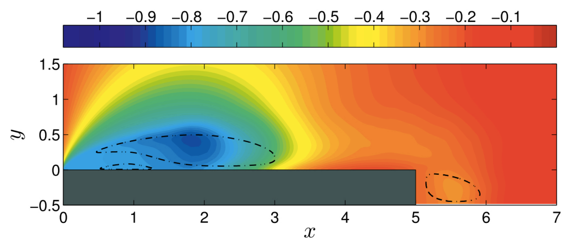

Fig. 28 DNS square cylinder mean pressure distribution Re=3000 [24]

Fig. 5. Isocontours of the mean pressure field P(x,y). The dashed lines report the location of the primary vortex, secondary vortex and wake vortex.

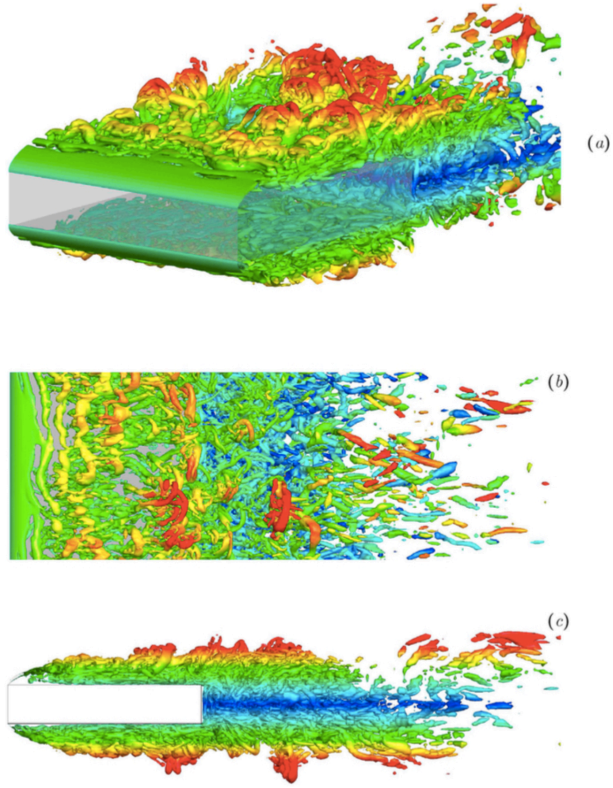

Fig. 29 DNS square cylinder vorticity contours Re=3000 [24]

Fig. 10. Instantaneous isosurfaces of $\lambda_2 = -2$ colored with y. Perspective, top and lateral views in (a), (b) and (c) plots, respectively.

VI. Current State of Bluff-Body Turbulence Analysis

- Current State of Knowledge
- Remaining Challenges

A. Experimental Methods

FZ

B. Computational Methods

LH

VII. Conclusions

LH&FZ

Acknowledgments

LH&FZ

Example citations

[25]

References

[1] Elkhoury, M., "Assessment of turbulence models for the simulation of turbulent flows past bluff bodies," *Journal of Wind Engineering and Industrial Aerodynamics*, Vol. 154, 2016, pp. 10 – 20. doi:https://doi.org/10.1016/j.jweia.2016.03.011, URL http://www.sciencedirect.com/science/article/pii/S0167610515300945.

[2] Yuan, W., Laima, S., Chen, W., Li, H., and Hu, H., "Investigation on the vortex-and-wake-induced vibration of a separated-box bridge girder," *Journal of Fluids and Structures*, Vol. 70, 2017, pp. 145 – 161. doi:https://doi.org/10.1016/j.jfluidstructs.2017.01.015, URL http://www.sciencedirect.com/science/article/pii/S0889974616304911.

[3] Mendonça, F., Allen, R., de Charentenay, J., and Lewis, M., "Towards Understanding LES and DES for Industrial Aeroacoustic Predictions," *International workshop on 'LES for Acoustics'*, DLR Göttingen, Germany, October 2002.

[4] Ross, J. C., Heineck, J. T., Burnside, N., Sellers, M. E., Halcomb, N., Garbeff, T., Yamauchi, G., and Kushner, L., "Comprehensive Study of the Flow Around a Simplified Orion Capsule Model," *31st AIAA Applied Aerodynamics Conference*, San Diego, CA, June 2013.

[5] Tanaka, S., Takahashi, K., Hosoi, J., and Uchida, M., "Bluff Body Flame Holder with Flow Entrainment Using Perforated Plate," *9th AIAA/ASME/SAE/ASEE Joint Propulsion Conference*, San Jose, CA, July 2013.

[6] Li, H., Sung, H., and Yang, V., "Large Eddy Simulation of Combustion Dynamics of Bluff Body Stabilized Flame," *49th AIAA Aerospace Sciences Meeting including the New Horizons Forum and Aerospace Exposition*, Orlando, Florida, January 2011.

[7] Richardson, L. F., *Weather Prediction by Numerical Process*, Cambridge University Press, Cambridge, UK, 1922.

[8] Hunt, J., Kawai, H., Ramsey, S., Pedrizetti, G., and Perkins, R., "A review of velocity and pressure fluctuations in turbulent flows around bluff bodies," *Journal of Wind Engineering and Industrial Aerodynamics*, Vol. 35, 1990, pp. 49 – 85. doi:https://doi.org/10.1016/0167-6105(90)90210-4, URL https://www.sciencedirect.com/science/article/pii/0167610590902104.

[9] Zdravkovich, M., "Smoke obervations of the formation of a Kárman vortex street," *Journal of Fluid Mechanics*, Vol. 37, No. 3, 1968, pp. 491 – 496. doi:doi:10.1017/S0022112069000681, URL https://www.cambridge.org/core/journals/journal-of-fluid-mechanics/article/smoke-observations-of-the-formation-of-a-karman-vortex-street/C9BFB26B8A755EAFFFA6ACC3C91800FB.

[10] Gerrard, J. H., “The wakes of cylindrical bluff bodies at low Reynolds number,” *Philosophical transactions of the Royal Society A*, Vol. 288, 1978, pp. 351 – 382. doi:https://doi.org/10.1098/rsta.1978.0020, URL `http://rsta.royalsocietypublishing.org/content/288/1354/351.article-info`.

[11] Zdravkovich, M. M., “Flow around Circular Cylinders; Volume 1. Fundamentals,” *Journal of Fluid Mechanics*, Vol. 350, 1997, p. 375–378. doi:10.1017/S0022112097227291.

[12] Menter, F., and Egorov, Y., “A Scale Adaptive Simulation Model using Two-Equation Models,” *43rd AIAA Aerospace Sciences Meeting and Exhibit, Aerospace Sciences Meetings*, Reno, NV, January 2005.

[13] Catalano, P., Wang, M., Iaccarino, G., and Moin, P., “Numerical simulation of the flow around a circular cylinder at high Reynolds numbers,” *International Journal of Heat and Fluid Flow*, Vol. 24, No. 4, 2003, pp. 463 – 469. doi:https://doi.org/10.1016/S0142-727X(03)00061-4, URL `http://www.sciencedirect.com/science/article/pii/S0142727X03000614`, selected Papers from the Fifth International Conference on Engineering Turbulence Modelling and Measurements.

[14] Travin, A., Shur, M., Strelets, M., and Spalart, P., “Detached-Eddy Simulations Past a Circular Cylinder,” *Flow, Turbulence and Combustion*, Vol. 63, No. 1, 2000, pp. 293–313. doi:10.1023/A:1009901401183, URL `https://doi.org/10.1023/A:1009901401183`.

[15] Spalart, P., “Strategies for turbulence modelling and simulations,” *International Journal of Heat and Fluid Flow*, Vol. 21, No. 3, 2000, pp. 252 – 263. doi:https://doi.org/10.1016/S0142-727X(00)00007-2, URL `http://www.sciencedirect.com/science/article/pii/S0142727X00000072`.

[16] Spalart, P. R., “Detached-Eddy Simulation,” *Annual Review of Fluid Mechanics*, Vol. 41, No. 1, 2009, pp. 181–202. doi:10.1146/annurev.fluid.010908.165130, URL `https://doi.org/10.1146/annurev.fluid.010908.165130`.

[17] Squires, K. D., “Detached-Eddy Simulation: Current Status and Perspectives,” *Direct and Large-Eddy Simulation V*, edited by R. Friedrich, B. J. Geurts, and O. Métais, Springer Netherlands, Dordrecht, 2004, pp. 465–480.

[18] Mockett, C., Greschner, B., Knacke, T., Perrin, R., Yan, J., and Thiele, F., “Demonstration of Improved DES Methods for Generic and Industrial Applications,” *Advances in Hybrid RANS-LES Modelling*, edited by S.-H. Peng and W. Haase, Springer Berlin Heidelberg, Berlin, Heidelberg, 2008, pp. 222–231.

[19] Menter, F. R., and Kuntz, M., “Adaptation of Eddy-Viscosity Turbulence Models to Unsteady Separated Flow Behind Vehicles,” *The Aerodynamics of Heavy Vehicles: Trucks, Buses, and Trains*, edited by R. McCallen, F. Browand, and J. Ross, Springer Berlin Heidelberg, Berlin, Heidelberg, 2004, pp. 339–352.

[20] Schwing, A. M., and Candler, G. V., “Detached-Eddy Simulation of Capsule Wake Flows and Comparison to ind-Tunnel Test Data,” *Journal of Spacecraft and Rockets*, Vol. 52, No. 2, 2015, pp. 439–449.

[21] Forsythe, J. R., Squires, K. D., Wurtzler, K. E., and Spalart, P. R., “Detached-Eddy Simulation of the F-15E at High Alpha,” *Journal of Aircraft*, Vol. 41, No. 9, 2004, pp. 193–200.

[22] Durbin, P. A., "Some Recent Developments in Turbulence Closure Modeling," *Annual Review of Fluid Mechanics*, Vol. 50, No. 1, 2018, pp. 77–103. doi:10.1146/annurev-fluid-122316-045020.

[23] Smith, C., Beratlis, N., Balaras, E., Squires, K., and Tsunoda, M., "Numerical investigation of the flow over a golf ball in the subcritical and supercritical regimes," *International Journal of Heat and Fluid Flow*, Vol. 31, No. 3, 2010, pp. 262 – 273. doi: https://doi.org/10.1016/j.ijheatfluidflow.2010.01.002, URL `http://www.sciencedirect.com/science/article/pii/S0142727X10000147`, sixth International Symposium on Turbulence and Shear Flow Phenomena.

[24] Cimarelli, A., Leonforte, A., and Angeli, D., "Direct numerical simulation of the flow around a rectangular cylinder at a moderately high Reynolds number," *Journal of Wind Engineering and Industrial Aerodynamics*, Vol. 174, 2018, pp. 39 – 49. doi:https://doi.org/10.1016/j.jweia.2017.12.020, URL `http://www.sciencedirect.com/science/article/pii/S0167610517304622`.

[25] Nakamura, Y., "Bluff-body aerodynamics and turbulence," *Journal of Wind Engineering and Industrial Aerodynamics*, Vol. 49, No. 1, 1993, pp. 65 – 78. doi:https://doi.org/10.1016/0167-6105(93)90006-A, URL `http://www.sciencedirect.com/science/article/pii/016761059390006A`.